IEEE Access
Multidisciplinary : Rapid Review : Open Access Journal

Received 2 March 2024, accepted 16 March 2024, date of publication 28 March 2024, date of current version 5 April 2024.

Digital Object Identifier 10.1109/ACCESS.2024.3382821

RESEARCH ARTICLE

Energizing an IoT Sensor Using Regenerative Opposite Fringing Fields From an Embedded Communicating Patch Antenna

SUNDEEP KUMAR[1], (Graduate Student Member, IEEE), MANOJ KUMAR[1], ASHWANI SHARMA[1], (Senior Member, IEEE), AND IGNACIO JULIO GARCIA ZUAZOLA[2], (Senior Member, IEEE)

[1]Electrical Engineering Department, Indian Institute of Technology Ropar, Rupnagar, Punjab 140001, India
[2]School of Computing and Digital Media, London Metropolitan University, N7 8DB London, U.K.

Corresponding author: Ignacio Julio Garcia Zuazola (i.garciazuazola@londonmet.ac.uk)

This work was supported in part by London Met Transformation Fund 2023/24; and in part by the Science and Engineering Research Board (SERB), Department of Science and Technology, Government of India, under Grant CRG/2022/007257.

ABSTRACT An integrated, miniature, dual-purpose circular patch antenna is proposed for Simultaneous Wireless Information and Power Transmission (SWIPT). The design proposes a proximity-coupled feed to the radiative circular patch for Wireless Information Transfer (WIT) in 5.7 GHz - 6.0 GHz band and an integrated capacitive-coupled feeding network, with full-wave rectification (FWR) using regenerative opposite fringing fields from the radiating edges of the patch for energizing IoT sensors by means of wireless power transfer (WPT) at 5.2 GHz. For the realization, two co-polarized fringing field harvesters are capacitively coupled to the radiating edges of the patch to regenerate those opposite fringes whose currents are effectively matched to the FWR using a pair of Schottky diodes for direct current (DC) power generation. Since the gain and efficiency of the patch, in WIT mode, are favoured when using the FWR network, the effective regenerative fields, which are deemed attractive in modern wireless sensor network (WSN) applications for boosting the lifespan of sensor nodes.

INDEX TERMS WPT, WIT, FWR, IoT, SWIPT, patch antennas.

I. INTRODUCTION

The 6G communication network is witnessing the increasing deployment of many sensor nodes specially in smart applications [1]. Different energy harvesting (EH) methods are being researched to enhance the battery lifespan of the sensor nodes. A wireless power transfer (WPT) technique has emerged as the most popular choice [2], [3] as it provides easy integration with the existing communication circuitry. Moreover, sensor nodes collect information related to the surrounding environment and communicate it with a remote gateway through an in-housed wireless information transfer (WIT) antenna. However, housing two separate antenna modules for WPT and WIT respectively, would render to a bulky prototype. To smaller their size, several research works have recently been reported towards implementing simultaneous wireless information and power transmission (SWIPT) to achieve concurrent data and power transfer to remote sensor nodes [4].

To realize SWIPT operation, several techniques can be employed, such as power splitting [5], [6], [7], time splitting [5], dual polarization [8], [9], frequency splitting [10], and space splitting [11], [12]. The power-splitting technique divides the received signal into two power ratios, one for information decoding and and the other one for radio frequency (RF) power harvesting, as shown in Fig. 1(a). However, this reduces the signal-to-noise ratio (SNR) as well as the power conversion efficiency (PCE) of the rectifier circuit. In contrast, the time-splitting technique, depicted in Fig. 1(b) allows, in principle, full RF signal power with better SNR and PCE, since different time slots are used for the information and the power transfer delivery. However, the

The associate editor coordinating the review of this manuscript and approving it for publication was Chan Hwang See.

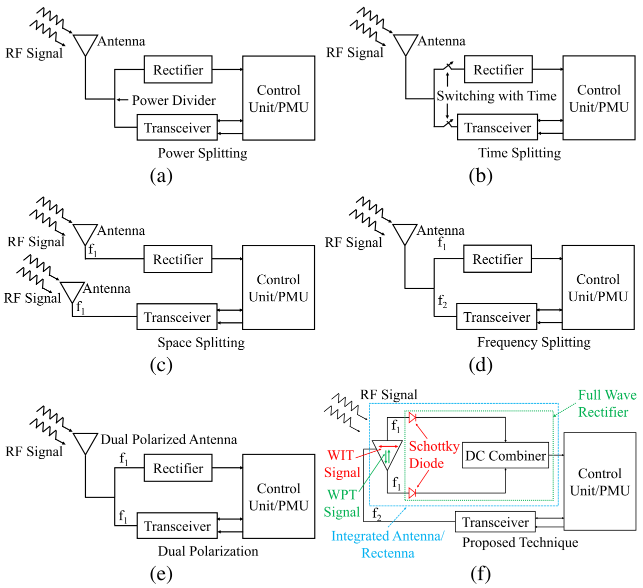

FIGURE 1. (a)-(e) Different SWIPT Techniques in literature, and (f) the one presented in this work.

major drawback of this technique is the time-synchronization need between the transmitter and the receiver [13]. Moreover, the optimal time divisions for many sensor nodes are different to achieve sustainable IoT operation. On the other hand, the space-splitting technique, Fig. 1(c) employs separate antenna elements for WIT and WPT operations at the same frequency of operation. In contrast, the frequency splitting technique, Fig. 1(d) utilizes different frequency channels for the information and the power transfer [10], [14], [15] whereas, in dual-polarization [8], [9], [16] technique, Fig. 1(e), cross-polarized ports are employed at the same frequency of operation. Further, a few hybrid SWIPT antenna systems are reported in the literature. For instance, a shared aperture antenna [17] with frequency splitting, a dual-polarized full-duplex antenna [18], [19], and a frequency splitting with dual-polarization [14] are proposed. However, these designs either use multiple antenna elements [17], [18], [19] or a rectifier impedance matching network [14], which results in bulky sensor nodes. In contrast, the frequency splitting and dual-polarization techniques are relatively easier to implement as they employ distinct frequency channels and orthogonal polarization for the information and power transfer, respectively. This enables high isolation between the WIT and WPT ports, resulting in improved SNR and PCE of the SWIPT antenna. In SWIPT systems, antenna and rectifier circuit are matched either using an impedance matching network (IMN) [14], [15] or employing loop-based conjugate matching techniques [8], [10], [16]. However, the latter requires partial ground plane which affects the antenna characteristics [20] when the IoT sensor node is placed on platforms of different dielectric properties. In addition, conjugate-matched SWIPT antennas [8], [16] employ a voltage doubler topology for full-wave rectification (FWR), achieving an enhanced PCE ($\sim$ 70%) at high input RF power ($\geq$ 500 μW) [21]. However, realizing FWR for ultra-low power (-10 dBm) [22] applications with such a high PCE poses a significant challenge [10]. Moreover, ultra-low power RF transmission is desired in IoT applications where human exposure to radiation satisfies the specific absorption rate (SAR) limit of 1.6 W/kg for their health and safety protection. Therefore, a miniature integrated antenna having high WIT efficiency and high PCE for ultra-low power WPT is desired for SWIPT applications. Here, an additional SWIPT technique is presented in Fig. 1(f), where a SWIPT single antenna system uses frequency splitting and dual polarization techniques, resulting in an integrated, miniature, dual-purpose circular patch antenna. The proposed design incorporates a proximity coupled feed to the radiative circular patch for WIT in 5.7 GHz-6.0 GHz band and an integrated capacitive coupled feeding network, with FWR, using regenerative opposite fringing fields from the radiating edges of the patch to energize IoT sensors through WPT at 5.2 GHz frequency channel. For the realization, two co-polarized fringing field harvesters are capacitively coupled to the radiating edges of the patch to regenerate those opposite fringes whose currents are effectively matched to the FWR using a pair of Schottky diodes for DC energy generation.

The remaining of the manuscript is divided into five sections. Section II presents the proposed SWIPT antenna design, including the system's architecture, the design evolution and simulated results. The antenna fabrication and measurement results are discussed in Section III to validate the design. Section IV presents a detailed performance comparison of the proposed antenna with the state-of-the-art designs. The relevance of sustainability is discussed in Section V and conclusion in Section VI.

II. PROPOSED SWIPT ANTENNA DESIGN AND SIMULATION

A. SYSTEM ARCHITECTURE

A 50 Ω antenna for WIT at 5.8 GHz (5.7 GHz - 6 GHz) [23], with a bore-sight radiation pattern is targeted first. It is followed by a direct conjugate-matched, dc-combined, to fully integrate within the same structure for WPT with optimum PCE at 5.2 GHz, since low frequencies achieve greater transmission distances (Friis equation) [10]. High isolation between the WIT and WPT is important since the information signal can leak power into the rectifier circuit due to mutual coupling; low isolation reduces the information signal strength, resulting in low communication link quality. A typical application scenario for the proposed SWIPT antenna is illustrated in Fig. 2, which shows a SWIPT-enabled IoT sensor node informing wirelessly sensed data either directly through a remote gateway or a mobile drone communication relay. These sensor nodes can harvest RF power from a locally installed static or mobile drone power beacons and be used in vast IoT applications,

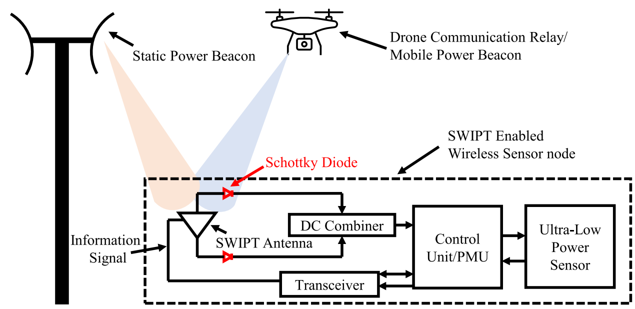

FIGURE 2. Application scenario for the proposed SWIPT antenna.

including smart homes, smart warehouses, smart farming, smart transportation, etc.

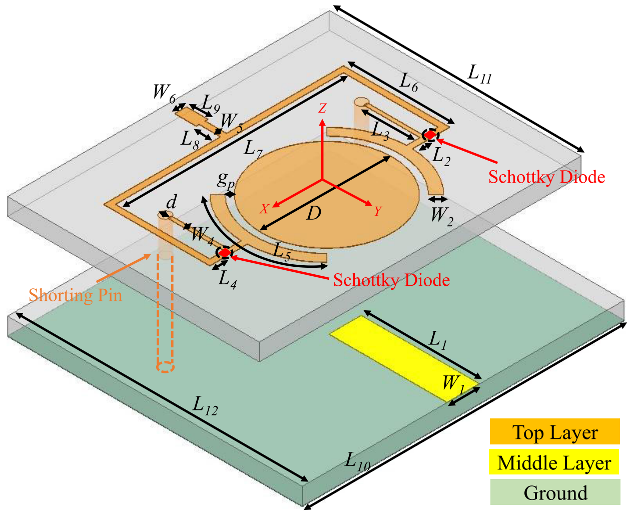

FIGURE 3. Exploded view of the proposed SWIPT antenna.

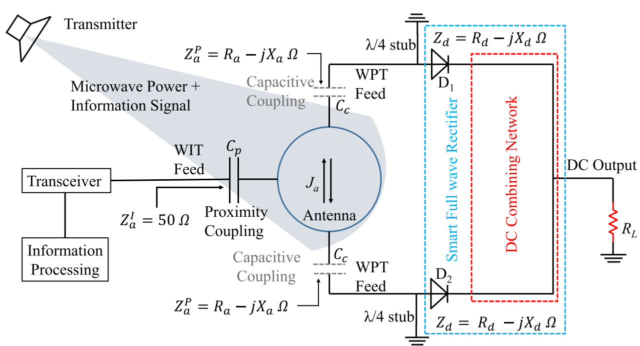

FIGURE 4. Equivalent circuit diagram of the proposed SWIPT antenna.

B. DESIGN AND LAYOUT

The proposed antenna is designed using Ansys HFSS on FR4 substrate ($\epsilon_r = 4.4$, $\tan\delta = 0.02$) having 1.6 mm thickness with 35 μm copper cladding. The rectifier circuit analysis is carried out in advanced design system (ADS) software. The final design layout is given in Fig. 3, indicating various design parameters listed in Table 1. The equivalent circuit diagram of the proposed SWIPT antenna is shown in Fig. 4, detailing its working mechanism. The capacitor C_p represents the proximity coupled WIT feed with $Z_a^I = 50\ \Omega$ input port impedance which can be connected to the transceiver for WIT post processing. Two co-polarized fringing field harvesters are capacitively coupled to the patch and represented by capacitors C_c with an input port impedance ($Z_a^p = R_a + jX_a\ \Omega$) that is conjugately matched to the Schottky diode impedance ($Z_d = R_d - jX_d\ \Omega$), which acts as an RF choke by inhibiting DC backflow to the antenna while permitting the integration of the FWR to the circular patch. The WPT feed lines are orthogonal with respect to the WIT feed to achieve high isolation between the WIT and the WPT signals. In Fig. 4, from a transmitter RF waves impinging on the SWIPT antenna generate TM_{110} mode current on the circular patch surface. The current direction, denoted by J_a (Fig. 4), changes in each subsequent half cycle of the incident RF wave and is noted with two arrows in opposite direction. Therefore, to convert the RF power every half cycle into usable DC energy, the two Schottky diodes are connected in mirror symmetry (diode's anode facing to the circular patch) with respect to the circular patch center.

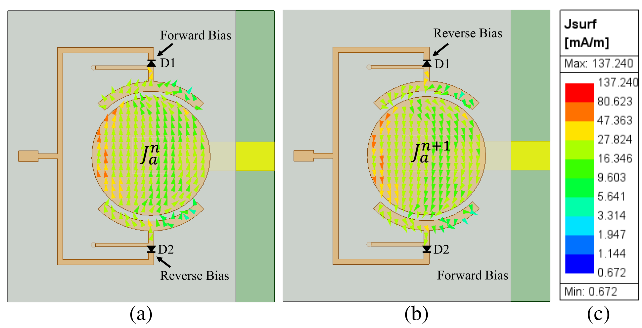

FIGURE 5. Current distribution on the proposed SWIPT antenna for (a) forward bias of D1, (b) forward bias of D2, and (c) range.

Fig. 5 shows the current distribution in the SWIPT antenna when diodes D_1 and D_2 are in excitation. Fig. 6 shows the working principle of the FWR by voltage sources V_{D1-D2} having an internal impedance of R_{D1-D2}. The surface current is excited (J_a^n) in patch antenna during the n^{th} half cycle of incident RF wave forward bias Schottky diode D_1. In the next $(n+1^{th})$ half cycle, the surface current (J_a^{n+1}) flows in reverse direction to J_a^n, forward biasing Schottky diode D_2. In reverse bias conditions, the Schottky diode does not contribute to the dc output and acts as an open load, indicating high S_{21} and S_{12} isolation between the ports. Further, the cathode terminals of both diodes are joined together through dc connection lines to combine output dc voltage in subsequent half cycles. This dc terminal grounds through an output load (R_L) using a $\lambda/4$ short stub connected to the anode of each Schottky diodes to provide necessary isolation between the RF signal and dc output as well as suppress even order harmonics that are generated by the Schottky diodes [24]. Unlike other

TABLE 1. Dimensions of the proposed SWIPT antenna.

Parameters	W_1	W_2	W_3	W_4	W_5	W_6	L_1	L_2	L_3	L_4	L_5	L_6	L_7	L_8	L_9	L_{10}	L_{11}	L_{12}	D	d	g_p
Dimension (mm)	3	1	0.55	0.35	0.55	1.1	11	1.6	5.23	1.37	10.52	9.9	21.25	2	2	30	23.45	27.45	12.2	0.5	0.6

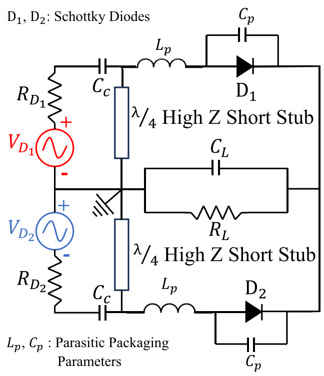

FIGURE 6. Working Principle of the FWR in the proposed SWIPT antenna.

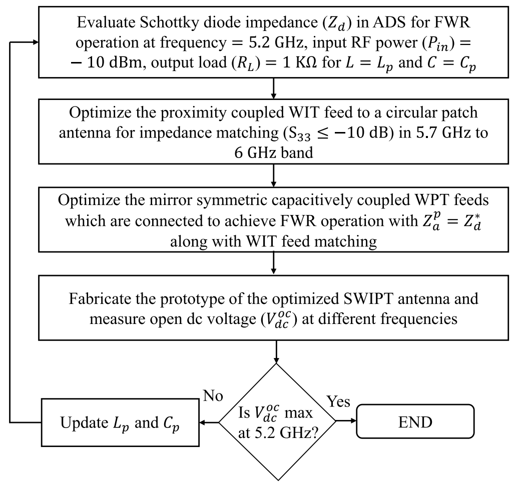

FIGURE 7. Detailed design procedure of the proposed SWIPT antenna.

literature, the proposed SWIPT antenna achieves FWR by dc combining a dual half-wave rectification (HWR) out of the two diodes that are integrating two co-polarized ports of a single circular patch antenna. The step-by-step design process with a detailed explanation of the evolution of the proposed SWIPT antenna is discussed in the subsequent subsection.

C. CIRCUIT SIMULATION AND DESIGN EVOLUTION

The analysis of non-linear rectifier circuit (SMS7621 − 079LF Schottky diode) is conducted using the harmonic balance (HB) technique and large signal S-Parameter (LSSP) technique in the advanced design system (ADS) software. These specific techniques facilitate the characterization of the nonlinear current-voltage characteristics of the diode through Fourier series expansion. The SMS7621 − 079LF Schottky diode was employed for the rectifier circuit due to its low junction capacitance, high cutoff frequency, and excellent power threshold sensitivity for low incoming RF signals [25]. The Schottky Diode SPICE parameters from the manufacturer's data sheet [26] allowed us to model it in ADS while iteratively accounting for the parasitic packaging parameters (L_p, C_p) when the input RF power was −10 dBm at 5.2 GHz frequency. That set the input impedance ($Z_d = 25 - j75\ \Omega$) for the design. The 1 kΩ resistance was taken as reference load to conjugate match the antenna's impedance with the Schottky diode impedance [27]. Corresponding to this impedance, the proposed SWIPT antenna was optimized in Ansys HFSS with conjugate impedance matching with Schottky diode impedance. This approach was selected to reduce insertion losses and the footprint of the overall SWIPT system. The detailed design procedure is elaborated using a flowchart in Fig. 7. To start the design process the initial value of L_p is taken as 3.7 nH which is the addition of packaging inductance of the Schottky diode (0.7 nH) and the series

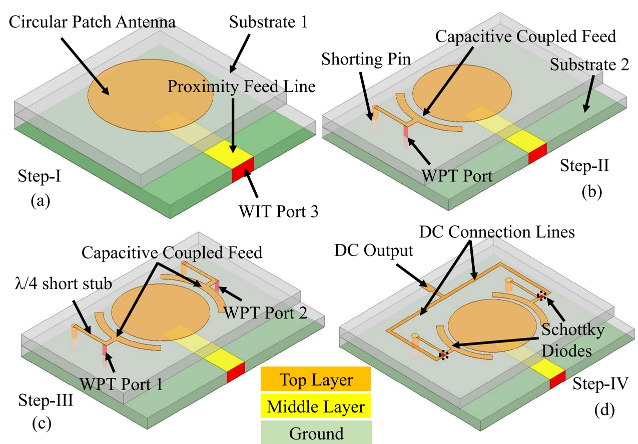

FIGURE 8. Design evolution of the proposed SWIPT antenna.

inductance due to the dc combining circuit (∼ 3 nH). On the other hand, the initial value of C_p is taken as 0.15 pF. The considered range for L_p and C_p are 3.5 nH to 4 nH and 0.05 pF to 0.15 pF, respectively, resulting in twenty five iterations of the design process to achieve the conjugate impedance matching at 5.2 GHz. The design evolution of the proposed SWIPT antenna is illustrated in Fig. 8. The proposed antenna comprises a three-layer structure implemented using two FR4 substrates (substrate 1 and substrate 2) to achieve wider impedance matching for WIT. Moreover, a circular patch geometry was preferred as the main radiator as it possesses the natural ability to reject harmonics (nf_0, $n \in \mathbb{Z}$) generated by diodes, since it resonates at frequencies that are non-integer ($n \notin \mathbb{Z}$) order [28] of the fundamental frequency. Initially (Step-I), the patch was excited with a

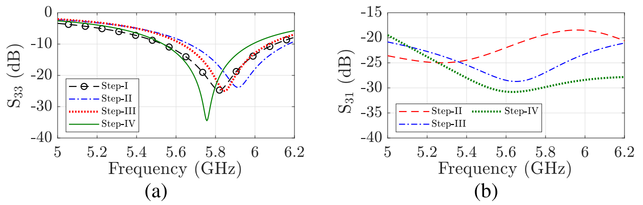

FIGURE 9. (a) Simulated reflection coefficient (S_{33}) of the WIT Port, and (b) Isolation (S_{31}) between the WIT and WPT ports at various design evolution stages of the proposed SWIPT antenna.

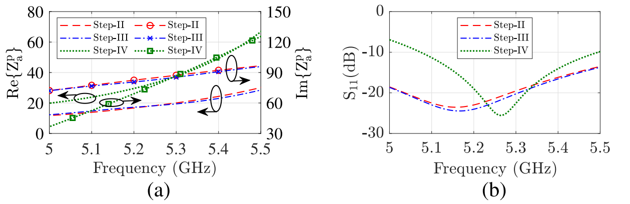

FIGURE 10. (a) Real and Imaginary part of the WPT port input impedance and respective (b) S_{11} at various design evolution stages of the proposed SWIPT antenna.

proximity-coupled microstrip feed line for WIT as illustrated in Fig. 8(a). The antenna design parameters were then optimized to achieve the desired impedance (Z_a^I) bandwidth (5.7 GHz-6 GHz) and is demonstrated in Fig. 9 (a) for each evolution step. In step-II, a capacitively coupled WPT feed was cross-polarized with respect to the WIT feed, as shown in Fig. 8(c). This arrangement achieved high isolation between information (WIT) and power signals (WPT) greater than 23 dB as confirmed in Fig. 9 (b). Moreover, the capacitive coupling technique [29], between the WIT and the WPT, inhibited dc back-flow into the antenna's radiator and enabled good conjugate impedance matching between the antenna's radiator (Z_a^P) and the dc rectifier circuit (Z_d). A $\lambda/4$ high impedance short stub transformer [30] was employed to choke RF signal flowing into the ground while passing dc from the rectifier to the output load (R_L). In step-III, shown in Fig. 8 (c), an additional co-polarized WPT port 2 was incorporated by connecting a Schottky diode in mirror symmetry to the one connected to WPT port 1. In the final step-IV, the dc outputs from both WPT ports 1 and 2 (Fig. 8 (c)) are meticulously brought into a single DC Output terminal using a microstrip line combiner, Fig. 8 (d), to achieve a FWR, as described in earlier section II-B. Fig. 10 (a) shows the real and imaginary part of the WPT port input impedance at various design evolution stages of the proposed SWIPT antenna. Fig. 10 (b) illustrates the corresponding impedance matching (S_{11}) of the WPT port using (1)

$$S_{11} = 20\log_{10}\left|\frac{Z_a^p - Z_d^*}{Z_a^p + Z_d^*}\right| \tag{1}$$

for determining the optimal matching of the FWR network. That favored an integrated, miniature, dual-purpose circular patch antenna operating between 5.7 GHz - 6.0 GHz for SWIPT using the proximity coupled feed to the radiative circular patch for WIT. The integrated capacitive coupled feeding network, with FWR, allow to regenerate the opposite fringing fields from the radiating edges of the patch for energizing IoT sensors by means of WPT.

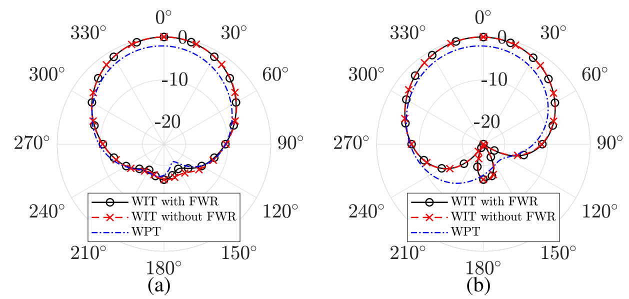

FIGURE 11. Simulated radiation pattern (normalized) of the WIT (with and without FWR) and WPT, for (a) $\phi = 0°$, and (b) $\phi = 90°$ elevation plane at 5.8 GHz and 5.2 GHz, respectively.

D. SIMULATION RESULTS AND DISCUSSION

The simulated S_{11} of the circular patch antenna (the WIT) is shown in Fig. 9 (a) (Step-IV curve). It shows an impedance bandwidth between 5.53 GHz - 6.0 GHz for WIT. In addition, the tailored SWIPT antenna geometry (Table 1) allowed the input impedance of the WPT ($29.67 + j69.43$) Ω to optimally conjugate match the FWR network ($25 - j75$) Ω covering dual-purpose applications in SWIPT. Furthermore, an isolation (S_{21}) of 24 dB at WPT frequency and ≥ 28 dB in the entire WIT band of operation is achieved as illustrated in Fig. 9 (b) (Step-IV curve). This helps inhibiting the leakage of information signal from the WIT into the FWR network for improved SNR communications while regenerating the opposite fringing fields from the radiating edges of the patch for energizing IoT sensors. The simulated radiation patterns (normalized) of the SWIPT antenna in the WIT and WPT modes are depicted in Fig. 11 (a) and Fig. 11 (b), respectively. Results show 5.7 dBi and 3.65 dBi, respectively for the WIT (with and without FWR) and WPT. The $\phi = 0°$ and $\phi = 90°$ elevation plane patterns for the proposed SWIPT antenna in the WIT mode (WPT mode) have 3 dB beamwidth of 84° and 92° (100° and 108°), respectively. That corresponded to a high radiation efficiency of 80.97% for the WPT operation at 5.2 GHz and > 78% for the WIT operation (with and without FWR).

III. ANTENNA FABRICATION AND MEASUREMENT

A. FABRICATION AND MEASUREMENT SETUP

The proposed SWIPT antenna was fabricated using a MITS PCB prototyping machine. The detailed description of the prototyped antenna is given in Fig. 12. The WIT mode performance was measured using a Keysight PNA-L (N5234B) VNA. All the measurements were carried out in an anechoic chamber as illustrated in Fig. 13(a). To measure the WPT mode performance, a horn antenna was used as a transmitter (Tx) and fed by an RF signal generator. The proposed SWIPT antenna was mounted on the turn table and

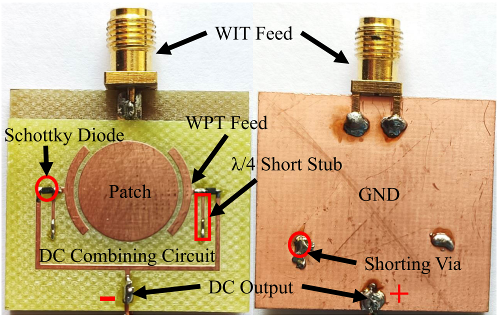

FIGURE 12. Fabricated prototype of the proposed SWIPT antenna.

at d distance from the Tx horn antenna. The received RF power at the antenna aperture was measured using a Keysight spectrum analyzer (N9951A), and the harvested dc voltage measured across the dc output terminals (Fig. 12) using a Keysight multimeter (U1232A). The WPT measurements are carried out in an anechoic chamber as shown in Fig. 13(b). A detailed description of the WPT link budget used in the measurements is listed in Table 2.

TABLE 2. Link budget parameters.

WPT Transmitter and Propagation Parameters	
Frequency (f)	5.2 GHz
RF Signal generator power (P_t)	25 dBm
Measured Cable Loss L_c	2.3 dB
Transmitter antenna (horn) gain (G_t)	10.5 dBi
EIRP ($P_t + G_t - L_c$)	33.2 dBm
Distance (d)	1 m

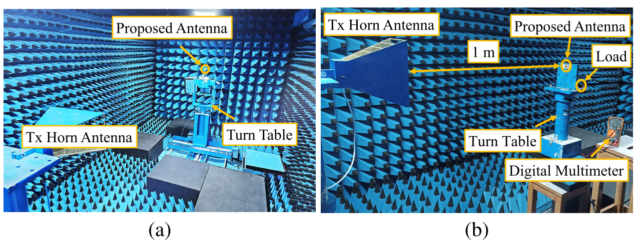

FIGURE 13. Experimental setup in an anechoic chamber for measuring (a) the proposed SWIPT antenna's radiation pattern, and (b) it's DC power pattern and PCE.

B. MEASUREMENT RESULTS AND DISCUSSION

1) IMPEDANCE MATCHING AND PATTERN MEASUREMENTS

The reflection coefficient (S_{33}) of the WIT port was measured by using Keysight PNA-L and is shown in Fig. 14. The measured S_{33} results reflect good agreement with simulation results for the proposed SWIPT antenna that achieves an impedance bandwidth of 5.7 GHz-6.0 GHz. The conjugate impedance matching poses difficulties in measuring FWR impedance on the Vector Network Analyzer (VNA) in the absence of a balun probe. As an alternative to validate the conjugate impedance matching of the FWR circuit, harvested

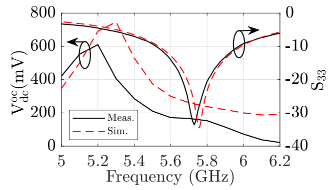

FIGURE 14. Measured reflection coefficient (S_{33}) port and output open dc voltage $\left(V_{dc}^{oc}\right)$ of the proposed SWIPT antenna.

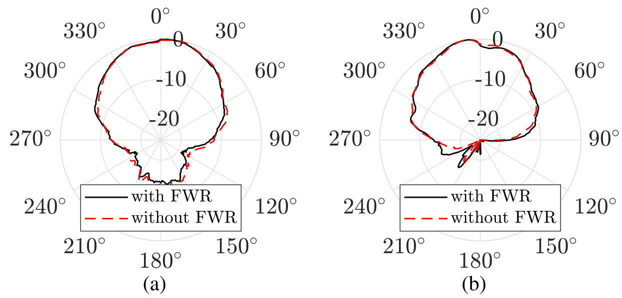

FIGURE 15. Measured radiation patterns (normalized) of the WIT in (a) $\phi = 0°$, and (b) $\phi = 90°$ elevation plane at 5.8 GHz with and without Schottky diode.

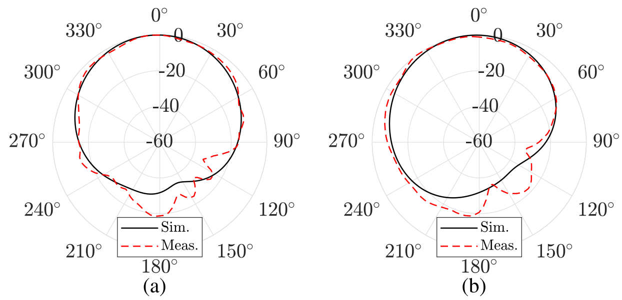

FIGURE 16. Simulated and Measured dc power patterns (normalized) of WPT in (a) $\phi = 0°$, and (b) $\phi = 90°$ elevation plane at 5.2 GHz.

open dc voltage $\left(V_{dc}^{oc}\right)$ is measured for input RF signals ranging from 5 GHz-6.2 GHz using the measurement setup shown in Fig. 13. The results shown in Fig. 14 illustrate voltage maxima (610.2 mV) at 5.2 GHz, demonstrating precise impedance matching of the FWR at the desired frequency and in agreement with the simulated WPT port impedance matching (S_{11}) given in Fig. 10 (b) (Step-IV curve). The measured radiation patterns of the WIT are depicted in Fig. 15, revealing a commendable alignment with the simulation results presented in Fig. 11. The results indicate a very insignificant effect of the Schottky diode on the radiation patterns, and gains of 5.65 dBi and 5.57 dBi is noted with and without the FWR network. The measured $\phi = 0°$ and $\phi = 90°$ elevation plane patterns (for the WIT) have 3 dB beamwidths of 66.7° and 75.6°, respectively. The slight deviation between the measured and the simulated results can be attributed to fabrication errors. To verify the simulated radiation patterns, open dc voltage are measured. The output dc power is proportional to input RF power and the rectifier efficiency [31, eq. (3)] which is also a function of the input RF power [31, eq. (4)]. Thus, simulated output dc power is proportional to the square of the input RF power and is equivalent to the square of the radiation pattern gain. In Fig. 16 comparison between the measured and simulated dc power patterns are shown, which are in fair agreement.

2) PCE MEASUREMENTS

The harvested dc voltage and PCE of the SWIPT antenna are measured using the measurement setup shown in Fig. 13(b). The received power (P_r) is evaluated using the Friis formula given in (2),

$$P_r(\text{dBm}) = \text{EIRP}(\text{dBm}) + G_r(\text{dBi}) + 20\log_{10}\left(\frac{\lambda}{4\pi d}\right) \tag{2}$$

where, G_r is the receiver realized antenna gain, and λ is the transmitting signal wavelength, EIRP is the effective isotropic radiated power and d the distance (Table 2). The evaluated P_r is later validated through measurement by the spectrum analyzer for complete characterization of the WPT. Using the setup of Fig. 13(b) and the link budget of Table 2, the P_r for the proposed SWIPT antenna was −9.91 dBm. Results with a varied range between −19 dBm to −9 dBm and varied output load (R_L) of the WPT is plotted in Fig. 17(a) which indicates a maximum PCE of 66.52% with 203.5 mV output dc voltage $\left(\text{V}_{\text{dc}}^{\text{R}_\text{L}}\right)$ at an optimal load of 610 Ω corresponding to measured dc power (P_{dc}) of 67.9 µW. The P_{dc} can be evaluated from the $V_{dc}^{R_L}$ plots shown in Fig. 17 using (3) and from PCE plots in Fig. 18 using (4).

$$P_{dc}(\mu\text{W}) = \frac{\left(V_{dc}^{R_L}\right)^2}{R_L} \tag{3}$$

$$P_{dc}(\mu\text{W}) = \frac{\%PCE}{100} \times 10^{\left(\frac{P_r(\text{dBm})}{10}\right)} \times 10^3 \tag{4}$$

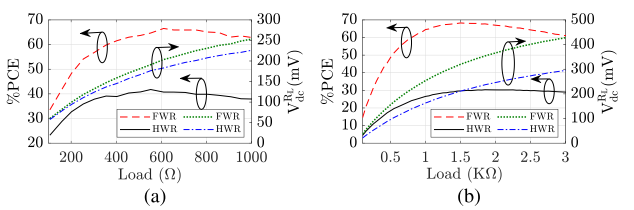

FIGURE 17. (a) Measured and (b) Simulated PCE and harvested DC voltage of the WPT vs the load.

Moreover, one Schottky diode was removed to compare the PCE response for a HWR vs the FWR of the proposed SWIPT antenna. Since the SWIPT antenna was designed for FWR, the diode removal resulted in a upshifted impedance matching frequency to 5.56 GHz, G_r of 5.44 dBi and P_r = −8.7 dBm. A maximum PCE of 41.76% at 552.7 Ω load in Fig. 17 (a) indicates a significant PCE improvement for the FWR configuration. The simulated output dc voltage and PCE for various output load (R_L) are shown in Fig 17(b) respectively, indicating a maximum efficiency of 68.3% (30.2%) for FWR (HWR) at 1.5 kΩ (1.75 kΩ) for an input RF power of −10 dBm at 5.2 GHz. The measured and simulated PCE with varied input RF power is given in Fig. 18 (a) and Fig. 18 (b), respectively. The results show a non-linear increase in PCE and output dc voltage with respect to the input RF power. This input RF power corresponds to the non-linear $I - V$ characteristics of the Schottky diode. The difference in the measured and simulated results can be attributed to the different input RF power levels and optimal output load R_L.

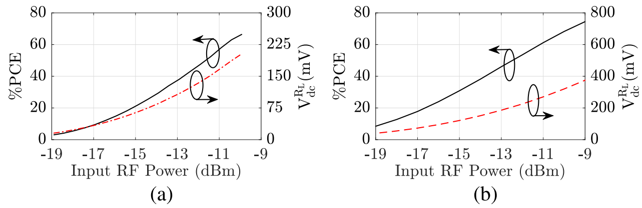

FIGURE 18. (a) Measured and (b) Simulated PCE and harvested DC voltage of the WPT vs input RF power at 5.2 GHz for 610 Ω and 1.5 KΩ, respectively.

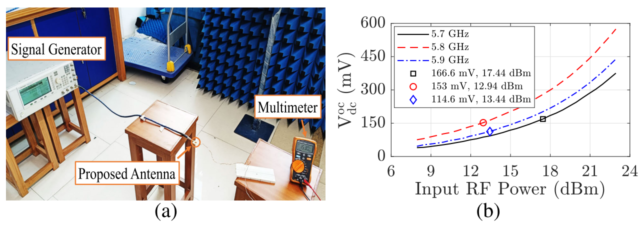

FIGURE 19. (a) Experimental setup to measure isolation between WIT and WPT port of the proposed SWIPT antenna, (b) Measured output open dc voltage vs RF power input to WIT feed.

3) ISOLATION MEASUREMENTS

The isolation between the WIT and WPT ports is validated using a two-step measurement process. In the first step, the proposed SWIPT antenna is incident with a 5.7, 5.8, and 5.9 GHz RF signal using the measurement setup illustrated in Fig. 13 (b) and the corresponding output open dc voltages (V_{dc}^{oc} = 166.6, 153, and 114.6 mV). That gave a P_r (−8.81, −8.92, and −9.2 dBm) at the antenna aperture using (2). In the next step, the WIT feed of the proposed SWIPT antenna was directly connected to the signal generator using an RF cable of L_c = 1.6 dB loss as shown in Fig. 19 (a). The output V_{dc}^{oc}, generated due to coupling between the WPT and the WIT ports was measured using a multimeter at several frequencies. The results are plotted in Fig. 19(b) for effective P_r ranging from 7.94 dB to 22.94 dB. The results indicate 153 mV open dc voltage for 12.94 dBm RF input at 5.8 GHz, suggesting coupling of −8.92 dBm power and 12.94 + 8.92 = 21.86 dB isolation between WIT and WPT ports. Similarly, the isolation at 5.7 GHz and 5.9 GHz were 26.25 dB and 21.64 dB, respectively. The measurement results show a fair agreement with the

TABLE 3. Performance comparison with state-of-the-art.

Parameters	[14]	[10]	[8]	[16]	[7]	[6]	[5]	This Work
Freq (GHz) WPT/WIT	5.8 / 6.1	0.868 / 2.4	2.4 / 2.4	2.4 / 2.4	5.8 / 5.8	5.2 & 5.73 / 5.2 & 5.73	2.4 / 2.4	5.2 / 5.8
WIT Gain (dBi)	7	7.2	5	8.4 - 9.6	$4.71 - 5.15$	$4.22 - 5.68$	$3.64 - 4.10$	5.7
WPT Gain (dBi)	7.2	1.7	6.4	2.5 - 4	$4.71 - 5.15$	$4.22 - 5.68$	$4.10 - 4.57$	3.6
Total WIT Efficiency	NG	63%	41%	$70\% - 88\%$	NG	NG	90.5%	$78\% - 80.23\%$
Min. Port Isolation (dB)	25	30	45	$10 - 16$	15	15	15	21.64
Input RF Power (dBm)	13.97	-9.5	3	2	0.5	5	6	-9.91
PCE @ -9.91 dBm	NG	60%	44%	55%	33%	$\leq 30\%$	NG	66.52%
DC Combining	No	No	No	No	No	No	No	Yes
Conjugate Matching	No	Yes	Yes	Yes	No	No	No	Yes
SWIPT Technique Employed	hybrid	freq split	dual-pol	dual-pol	power split	power split	either power split or time split	freq split + dual-pol + dc combine
Rectification Method	half wave	voltage doubler	voltage doubler	voltage doubler	half wave	half wave	half wave	full wave
Electrical size (λ_0 @ WIT freq)	$> 0.82 \times 1$	0.74×0.63	0.63×0.63	0.61×0.61	2.5×10.6	$> 1.57 \times 1.05$	$> 0.984 \times 0.432$	0.58×0.53

Abbreviations:- NG: not given; freq: frequency; pol: polarization; split: splitting

simulated isolation results illustrated in Fig. 9 (b) and the small variations can be attributed to fabrication errors.

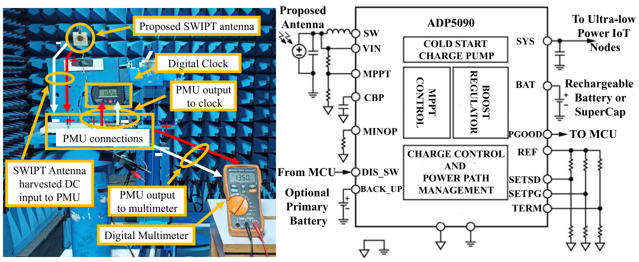

FIGURE 20. (a) Demonstration of the proposed SWIPT antenna for energizing IoT sensors, and (b) Configuration of the ultra low power boost regulator [32].

C. DEMONSTRATION OF PROPOSED SWIPT ANTENNA FOR ENERGIZING IOT SENSORS

A digital clock with voltage and current ratings of 1.1 V and 10 µA was set to the proposed SWIPT antenna for demonstration of energizing IoT sensors, as illustrated in Fig. 20. Since the voltage rating was set higher than the open voltage (610.2 mV) of the proposed SWIPT antenna, a power management unit (PMU) was combined with the SWIPT antenna as depicted in Fig. 20 (a). The PMU is ADP5090-2-EVALZ from Analog Devices which is a plug and play evaluation board for WPT [32]. The complete diagram is shown in Fig. 20 (b) and is an ultra-low power booster regulator incorporated with charge management and maximum power point tracking (MPPT) features to provide efficient conversion of the harvested power from 16 µW to 200 mW range [33]. Preliminary measurements corroborated the capability of the proposed SWIPT antenna to operate small IoT sensor nodes if integrated with an ultra-low PMU.

IV. PERFORMANCE COMPARISON WITH STATE OF THE ART

The performance of the proposed SWIPT antenna is compared in Table 3 with other state-of-the-art. The designs in [10] and [14] use frequency splitting for SWIPT operation, that achieves a high port isolation ($\geq$ 25 dB) utilizing cross-polarization [14] and dual-mode operation [10] for WIT and WPT. However, these prototypes have lower PCE and WIT efficiency than the proposed SWIPT antenna (Table 3). Moreover, the matching network in [14] is more bulky than the proposed one. For instance, the proposed SWIPT antenna is 34%-62.51% smaller than the designs presented in [10] and [14], respectively. Other state-of-the-art designs [5], [6], [7], [8], [16] deliver information and power at the same frequency. The linearly polarized design in [8] has cross-polarized WIT and WPT ports with isolation of 45 dB but with compromised WIT efficiency and PCE (Table 3). Similarly, in [16], cross-polarized ports are used with dual polarization features. However, the poor co-polarization and cross-polarization isolation (Table 3) between WIT and WPT indicate information signal leakage into the rectifier (the voltage doubler). The power split in [5], [6], and [7] requires a directional coupler, so that one of the output ports of the branch line coupler is connected to the rectifier with a matching network and a dc low pass filter (LPF) to achieve the WPT operation. This resulted in a large prototype with lower isolation and PCE compared to the proposed design. Furthermore, the reported state-of-the-art of Table 3 have a partial ground planes, thus, resulting in platform dependency since the antenna performance changes with the permittivity materials where it is placed. In summary, driven by the dual polarization [8], [16] and power splitting [5], [6], [7] techniques for an advanced SWIPT operation, a miniature integrated antenna having high WIT efficiency, high port isolation, high PCE (from FWR) for ultra-low power WPT is achieved for SWIPT applications (Table 3); making it suitable for integration with ultra-low power sensor nodes.

V. RELEVANCE TO SUSTAINABILITY

Future 6G communication systems aim at providing energy efficient and sustainable wireless sensor networks (WSN) [34]. Sensor nodes (including IoT) house small batteries limiting the lifespan of WSN and their large scale deployment increases the maintenance costs from vast battery replacements. Therefore, energy harvesting (EH) is envisioned as the indispensable technology component of 6G networks for realizing zero-energy wireless sensor nodes to deploy sustainable IoT applications.Therefore, the proposed SWIPT antenna uses a WPT technology that is perceived as the most suitable choice for EH due to its compact implementation [3] and easy integration with WIT communicating devices; energizing IoT sensors for battery waste/carbon foot print reduction with greener wireless communications.

VI. CONCLUSION

This paper proposes an integrated, miniature ($0.58\lambda_0 \times 0.53\lambda_0$), dual-purpose circular patch antenna for SWIPT. A proximity-coupled feed to the radiative circular patch for WIT operation between 5.7 GHz-6.0 GHz and an integrated capacitive-coupled feeding network with FWR is proposed to energize IoT sensor nodes through WPT with a Power Conversion Efficiency (PCE) of 66.52% at 5.2 GHz. The two co-polarized fringing field harvesters were capacitively coupled to the radiating edges of the patch to regenerate those opposite fringes. The corresponding currents were effectively matched to the FWR (−9.91 dBm sensitivity) using a pair of Schottky diodes for DC power generation. Since the gain and efficiency of the patch, in WIT mode, were favoured when using the effective regenerative fringing fields for the FWR network, making them deemed attractive in modern WSN applications for boosting the lifespan of sensor nodes.

REFERENCES

[1] C. D. Alwis, A. Kalla, Q.-V. Pham, P. Kumar, K. Dev, W.-J. Hwang, and M. Liyanage, "Survey on 6G frontiers: Trends, applications, requirements, technologies and future research," *IEEE Open J. Commun. Soc.*, vol. 2, pp. 836–886, 2021.

[2] M. Kumar, S. Kumar, and A. Sharma, "Dual-purpose planar radial-array of rectenna sensors for orientation estimation and RF-energy harvesting at IoT nodes," *IEEE Microw. Wireless Compon. Lett.*, vol. 32, no. 3, pp. 245–248, Mar. 2022.

[3] O. L. A. López, H. Alves, R. D. Souza, S. Montejo-Sánchez, E. M. G. Fernández, and M. Latva-Aho, "Massive wireless energy transfer: Enabling sustainable IoT toward 6G era," *IEEE Internet Things J.*, vol. 8, no. 11, pp. 8816–8835, Jun. 2021.

[4] T. D. P. Perera, D. N. K. Jayakody, S. K. Sharma, S. Chatzinotas, and J. Li, "Simultaneous wireless information and power transfer (SWIPT): Recent advances and future challenges," *IEEE Commun. Surveys Tuts.*, vol. 20, no. 1, pp. 264–302, 1st Quart., 2018.

[5] P. Lu, K. Huang, C. Song, Y. Ding, and G. Goussetis, "Optimal power splitting of wireless information and power transmission using a novel dual-channel rectenna," *IEEE Trans. Antennas Propag.*, vol. 70, no. 3, pp. 1846–1856, Mar. 2022.

[6] P. Lu, X.-S. Yang, and B.-Z. Wang, "A two-channel frequency reconfigurable rectenna for microwave power transmission and data communication," *IEEE Trans. Antennas Propag.*, vol. 65, no. 12, pp. 6976–6985, Dec. 2017.

[7] P. Lu, C. Song, and K. M. Huang, "A two-port multipolarization rectenna with orthogonal hybrid coupler for simultaneous wireless information and power transfer (SWIPT)," *IEEE Trans. Antennas Propag.*, vol. 68, no. 10, pp. 6893–6905, Oct. 2020.

[8] M. Wagih, G. S. Hilton, A. S. Weddell, and S. Beeby, "2.4 GHz wearable textile antenna/rectenna for simultaneous information and power transfer," in *Proc. 15th Eur. Conf. Antennas Propag. (EuCAP)*, Mar. 2021, pp. 1–5.

[9] L. Liao, Z. Li, Y. Tang, and X. Chen, "Dual-polarized dipole antenna for wireless data and microwave power transfer," *Electronics*, vol. 11, no. 5, pp. 1–9, 2022.

[10] M. Wagih, G. S. Hilton, A. S. Weddell, and S. Beeby, "Dual-band dual-mode textile antenna/rectenna for simultaneous wireless information and power transfer (SWIPT)," *IEEE Trans. Antennas Propag.*, vol. 69, no. 10, pp. 6322–6332, Oct. 2021.

[11] H. K. Sahu and P. R. Sahu, "SSK-based SWIPT with AF relay," *IEEE Commun. Lett.*, vol. 23, no. 4, pp. 756–759, Apr. 2019.

[12] S. Claessens, N. Pan, D. Schreurs, and S. Pollin, "Multitone FSK modulation for SWIPT," *IEEE Trans. Microw. Theory Techn.*, vol. 67, no. 5, pp. 1665–1674, May 2019.

[13] D. Kumar, O. L. Alcaraz López, S. K. Joshi, and A. Tölli, "Latency-aware multi-antenna SWIPT system with battery-constrained receivers," *IEEE Trans. Wireless Commun.*, vol. 22, no. 5, pp. 3022–3037, May 2023.

[14] X.-X. Yang, C. Jiang, A. Z. Elsherbeni, F. Yang, and Y.-Q. Wang, "A novel compact printed rectenna for data communication systems," *IEEE Trans. Antennas Propag.*, vol. 61, no. 5, pp. 2532–2539, May 2013.

[15] M. Ali, G. Yang, and R. Dougal, "A new circularly polarized rectenna for wireless power transmission and data communication," *IEEE Antennas Wireless Propag. Lett.*, vol. 4, pp. 205–208, 2005.

[16] M. Wagih, G. S. Hilton, A. S. Weddell, and S. Beeby, "Dual-polarized wearable antenna/rectenna for full-duplex and MIMO simultaneous wireless information and power transfer (SWIPT)," *IEEE Open J. Antennas Propag.*, vol. 2, pp. 844–857, 2021.

[17] J.-H. Ou, B. Xu, S. F. Bo, Y. Dong, S.-W. Dong, J. Tang, and X. Y. Zhang, "Highly-isolated RF power and information receiving system based on dual-band dual-circular-polarized shared-aperture antenna," *IEEE Trans. Circuits Syst. I, Reg. Papers*, vol. 69, no. 8, pp. 3093–3101, Aug. 2022.

[18] G.-L. Zhu, J.-X. Du, X.-X. Yang, Y.-G. Zhou, and S. Gao, "Dual-polarized communication rectenna array for simultaneous wireless information and power transmission," *IEEE Access*, vol. 7, pp. 141978–141986, 2019.

[19] Y.-M. Zhang and J.-L. Li, "A dual-polarized antenna array with enhanced interport isolation for far-field wireless data and power transfer," *IEEE Trans. Veh. Technol.*, vol. 67, no. 11, pp. 10258–10267, Nov. 2018.

[20] H.-M. Lee, "Effect of partial ground plane removal on the front-to-back ratio of a microstrip antenna," in *Proc. 7th Eur. Conf. Antennas Propag. (EuCAP)*, Apr. 2013, pp. 1204–1208.

[21] B. Clerckx, R. Zhang, R. Schober, D. W. K. Ng, D. I. Kim, and H. V. Poor, "Fundamentals of wireless information and power transfer: From RF energy harvester models to signal and system designs," *IEEE J. Sel. Areas Commun.*, vol. 37, no. 1, pp. 4–33, Jan. 2019.

[22] G. Pabbisetty, K. Murata, K. Taniguchi, T. Mitomo, and H. Mori, "Evaluation of space time beamforming algorithm to realize maintenance-free IoT sensors with wireless power transfer system in 5.7-GHz band," *IEEE Trans. Microw. Theory Techn.*, vol. 67, no. 12, pp. 5228–5234, Dec. 2019.

[23] Y.-X. Sun, K. W. Leung, and K. Lu, "Compact dual microwave/millimeter-wave planar shared-aperture antenna for vehicle-to-vehicle/5G communications," *IEEE Trans. Veh. Technol.*, vol. 70, no. 5, pp. 5071–5076, May 2021.

[24] T. Matsunaga, E. Nishiyama, and I. Toyoda, "5.8-GHz stacked differential rectenna suitable for large-scale rectenna arrays with DC connection," *IEEE Trans. Antennas Propag.*, vol. 63, no. 12, pp. 5944–5949, Dec. 2015.

[25] R. Trevisoli, H. P. D. Paz, V. S. D. Silva, R. T. Doria, I. R. S. Casella, and C. E. Capovilla, "Modeling Schottky diode rectifiers considering the reverse conduction for RF wireless power transfer," *IEEE Trans. Circuits Syst. II, Exp. Briefs*, vol. 69, no. 3, pp. 1732–1736, Mar. 2022.

[26] Skyworks Solutions, *Surface-Mount Mixer and Detector Schottky Diodes*, Standard SMS7621-079LF. Accessed: Oct. 2022.

[27] F. Erkmen, T. S. Almoneef, and O. M. Ramahi, "Electromagnetic energy harvesting using full-wave rectification," *IEEE Trans. Microw. Theory Techn.*, vol. 65, no. 5, pp. 1843–1851, May 2017.

[28] J. McSpadden and K. Chang, "A dual polarized circular patch rectifying antenna at 2.45 GHz for microwave power conversion and detection," in *IEEE MTT-S Int. Microw. Symp. Dig.*, vol. 3, May 1994, pp. 1749–1752.

[29] P. Lu, C. Song, and K. M. Huang, "A compact rectenna design with wide input power range for wireless power transfer," *IEEE Trans. Power Electron.*, vol. 35, no. 7, pp. 6705–6710, Jul. 2020.

[30] M. Kumar, S. Kumar, S. Jain, and A. Sharma, "A plug-in type integrated rectenna cell for scalable RF battery using wireless energy harvesting system," *IEEE Microw. Wireless Technol. Lett.*, vol. 33, no. 1, pp. 98–101, Jan. 2023.

[31] M. Kumar, S. Kumar, and A. Sharma, "An analytical framework of multisector rectenna array design for angular misalignment tolerant RF power transfer systems," *IEEE Trans. Microw. Theory Techn.*, vol. 71, no. 4, pp. 1835–1847, Apr. 2023.

[32] Analog Devices. *Ultralow Power Boost Regulator With MPPT and Charge Management*. Accessed: Dec. 2023. [Online]. Available: https://www.analog.com/media/en/technical-documentation/data-sheets/ADP5090.pdf
[33] Analog Devices. *ADP5090-2-EVALZ User Guide*. Accessed: Dec. 2023. [Online]. Available: https://www.analog.com/media/en/technical-documentation/user-guides/adp5090-2-evalzug-782.pdf
[34] A. A. Benbuk, N. Kouzayha, J. Costantine, and Z. Dawy, "Charging and wake-up of IoT devices using harvested RF energy with near-zero power consumption," *IEEE Internet Things Mag.*, vol. 6, no. 1, pp. 162–167, Mar. 2023.

SUNDEEP KUMAR (Graduate Student Member, IEEE) received the B.Tech. degree from the Career Institute of Technology and Management, Faridabad, India, in 2012, and the master's degree in electronics and communication engineering from the National Institute of Technology Kurukshetra, Kurukshetra, India, in 2019. He is currently pursuing the Ph.D. degree with the Department of Electrical Engineering, Indian Institute of Technology Ropar, Rupnagar, India. From 2013 to 2015, he was a Software Engineer with HCL Technologies Ltd., Chennai, India. His current research interests include antenna design for wireless power transmission, SWIPT, base stations, vehicular communication, the IoT, and 5G.

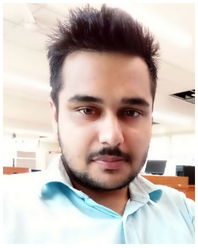

MANOJ KUMAR received the B.Tech. degree from Punjab Technical University, Kapurthala, India, in 2016, specializing in electronics and communication engineering, the M.Tech. degree from Kurukshetra University, Kurukshetra, India, in 2018, with a focus on RFID and meta-material antennas during this period, and the Ph.D. degree from IIT Ropar, where his research centered on smart antennas for the IoT applications. He has held the position of an Antenna Engineer with Wavelinks Antennas Technology, New Delhi, India, from 2017 to 2018. He was a Research and Development Engineer with Perfect RFID Private Ltd., Ghaziabad, India, from July 2018 to December 2018. He was a Solution Engineer with Agmatel. He is currently engaged with SLIET Longowal, where he contributes to the field by teaching digital system design in VLSI technology. He is a highly accomplished professional with a diverse academic and professional background in the field of electronics and communication engineering. His research interests include a wide array of areas, including rectenna design, meta-materials, RFID sensors, base station antenna design, the Internet of Things (IoT), 5G technology, RF-VLSI systems, and electric vehicles.

ASHWANI SHARMA (Senior Member, IEEE) received the B.Tech. degree from The LNM Institute of Information Technology, Jaipur, India, in 2010, the master's degree in technology and communication systems from Escuela Técnica Superior de Ingenieros de Telecomunicación (ETSIT), Technical University of Madrid (UPM), Madrid, Spain, in 2013, and the Ph.D. degree from the University of Deusto, Bilbao, Spain, in 2015. He was a Junior Research Fellow with IIT Delhi, New Delhi, India, from 2010 to 2011, and a Visiting Training Fellow with the University of Kent, Canterbury, U.K., from May 2014 to August 2014. He has been an Assistant Professor with IIT Ropar, Rupnagar, India, since July 2018. His research works have been published in various international journals and conferences, such as IEEE Transactions and Letters, IET journals, and Wiley letters. His current research interests include exploiting field-forming techniques in antenna design for wireless power transmission, the IoT, and 5G.

IGNACIO JULIO GARCIA ZUAZOLA (Senior Member, IEEE) received the F.P.I.I. degree in industrial electronics from the School of Chemistry and Electronics, Indautxu, Spain, in 1995, the H.N.D. degree in telecommunications engineering from the North West London–University of Middlesex, in 2000, the B.Eng. degree in telecommunications engineering from the Queen Mary University of London, in 2003, the Ph.D. degree in electronics (antennas) (part-time program) from the University of Kent, Canterbury, U.K., in 2010, and the M.B.A. degree in business (part-time program) from Cardiff Metropolitan University, U.K., in 2016. He has possesses the relevant industrial experience, been hired for Babcock & Wilcox, in 1993, Iberdrola, in 1995, Telefó nica, in 1997, Thyssen Elevators, in 1998, Cell Communications, in 2000, Nokia Bell Labs, in 2020, and Bilbao Ekintza, Bilbao City Council, in 2021. He engaged in a SME in electrical wiring, in 1996. In 2004, he has an academic experience and been employed as a Research Associate with the University of Kent, a Research Engineer (Grade 9/9) with the University of Wales, Swansea, U.K., in 2006, a Research Associate with the University of Kent, in 2008, a Senior Research Fellow with the University of Deusto, Bilbao, Spain, in 2011, a Visiting Senior Research Fellow with the University of Leeds, U.K., in 2011, a Research Associate with Loughborough University, U.K., in 2014, a Representative of Spain with London School of Commerce, U.K., in 2015, and a Lecturer in electronic engineering with the University of Portsmouth, U.K., in 2018. He was a Senior Lecturer with London Metropolitan University (London Met), U.K., in 2022. Included in Marquis Who's Who in the World 2010 Edition has been published in international journals: IEEE Transactions, IET Proceedings, and *Electronics Letters*. He led the antennas research line and supervised and mentored graduate and postgraduate students and currently bids for grants and contributes to the teaching, scientific, technological, and business development of London Met by promoting and increasing branding, research, and innovation. His current research interests include business development on one hand and single-band and multiband miniature antennas, and the use of electromagnetic-band gap (EBG) structures and frequency-selective surfaces (FSS). He is a MIET, a SMIEEE, and a SFHEA. He holds educational awards in electricity, pneumatic and hydraulics, and robotics.